Published in final edited form as:
Neuroimage. 2010 February 15; 49(4): 3149–3160. doi:10.1016/j.neuroimage.2009.10.087.

Changes in fMRI magnitude data and phase data observed in block-design and event-related tasks

Sunil Kumar Arja[a,b,*], **Zhaomei Feng**[a,b], **Zikuan Chen**[a], **Arvind Caprihan**[a], **Kent A. Kiehl**[a], **Tülay Adali**[c], and **Vince D. Calhoun**[a,b]

[a]The Mind Research Network, 1101 Yale Blvd NE, Albuquerque, NM 87131, USA

[b]Department of ECE, University of New Mexico, Albuquerque, NM, USA

[c]Department of CSEE, University of Maryland, Baltimore County, Baltimore, MD, USA

Abstract

Functional magnetic resonance imaging (fMRI) data are acquired as a complex image pair including magnitude and phase information. The vast majority of fMRI experiments do not attempt to take advantage of the time varying phase information. The phase of the MRI signal is related to the local magnetic field changes, suggesting it may contain useful information about the source of hemodynamic activity. Analysis of phase data acquired from different fMRI experiments has shown the presence of activity in response to various stimuli. However, there have been no studies that have examined phase data in a larger group of subjects for multiple types of fMRI tasks nor have studies examined phase changes due to event-related stimuli. In this paper, we evaluate the correspondence between the magnitude and phase changes at a group level in a block-design motor tapping task and in an event-related auditory oddball task. The results for both block-design and event-related tasks indicate the presence of task-related information in the phase data with phase-only and magnitude-only approaches showing signal changes in the expected brain regions. Although there is more overall activity detected with magnitude data, the phase-only analysis also reveals activity in regions expected to be involved in the task, some of which were not significantly activated in the magnitude-only analysis, suggesting that the phase might provide some unique information. In addition, the phase can potentially increase sensitivity within regions also showing magnitude changes. Future work should focus on additional methods for combining the magnitude and phase data.

Keywords

fMRI; BOLD; AOD; Phase changes

Introduction

Functional magnetic resonance imaging (fMRI) data are acquired as a complex image pair (or multiple pairs), with both the magnitude and the phase of signal. This complex-valued fMRI signal change has been shown to contain physiologic information (Hoogenraad et al., 2001). In spite of the presence of useful information in phase, it is usually discarded. Previous studies have reported task-related phase changes (Hoogenraad et al., 1998, 2001; Menon, 2002; Rowe, 2005b). Several approaches for modeling the phase have been proposed (Rowe, 2005a; Rowe and Logan, 2004, 2005). Processing complex-valued fMRI data using independent component

*Corresponding author. The Mind Research Network, 1101 Yale Blvd NE, Albuquerque, NM 87131, USA. arja@unm.edu (S.K. Arja).

analysis was also proposed in (Calhoun et al., 2002). Previous work has focused on filtering voxels with large phase changes (Menon, 2002; Nencka and Rowe, 2007; Tomasi and Caparelli, 2007; Zhao et al., 2007) based upon models that show that phase changes arise only from large non-randomly oriented blood vessels. More recent studies from our group and others provide evidence that the randomly oriented microvasculature can also produce a non-zero BOLD-related phase change (Feng et al., 2009; Zhao et al., 2007), suggesting that the phase information contains useful physiologic information. We evaluate the possibility of task-related phase changes in both block and event-related design studies and their correspondence with the regions expected to be involved in the tasks.

Previous research has reported phase changes in block-design tasks (Calhoun et al., 2002; Deshmukh et al., 20–22 Dec. 2004; Laird et al., 2002; Lee et al., 2007; Miller et al., 1–5 Sept. 2004; Petridou et al., 2009; Rowe and Logan, 2005; Weaver, 1999; Zhao et al., 2007) in single subjects, but to our knowledge no study has yet evaluated phase changes during an event-related design task, nor are we aware of any studies of phase changes evaluated at a group level. It is the goal of this paper to evaluate task-related phase changes compared to the task-related magnitude changes in both block-design tasks and event-related tasks. This paper particularly focuses on three main objectives, (a) evaluating the degree to which the voxels are activated in both phase and magnitude, (b) evaluating the degree to which the voxels showed only phase change or only magnitude change, and (c) evaluating whether phase changes can be detected in both block and event-related designs. In addition to addressing the three main objectives, the degree to which the active voxels occur in regions expected to be activated by the task are also evaluated.

In our paper, we analyze the phase changes across two different fMRI experimental paradigms (motor tapping and auditory oddball) via both region of interest analysis and whole brain analysis. The phase information is analyzed using a standard group analysis for both paradigms. We then compare the phase changes observed with those of the magnitude to observe the consistency of the phase signal change with that of magnitude. Throughout this paper, the phase data and the magnitude data are separately analyzed and the convergence of the results is evaluated. The identification of regions which (1) show signal changes for magnitude data only, (2) show signal changes for phase data only, or (3) show signal changes for both magnitude and phase data were of particular interest.

It is expected that by incorporating the phase information collected as a part of standard BOLD fMRI experiment, the analysis of whole brain BOLD fMRI data can be potentially improved. Our results are encouraging and suggest that further research should be conducted to better understand the phase data and to develop methods for integrating the phase data into the analysis pipeline.

Methods

fMRI subjects and paradigm

Subjects—Two data sets are analyzed for this paper. The first was data collected during a block-design motor tapping study and the second was data collected during an event-related auditory oddball task. For the motor tapping experiment, 20 healthy subjects participated in the motor tapping experiment, 17 subjects were right-handed, and 3 subjects were left-handed and in the age group between 18 and 62 years, with 12 male subjects and 8 female subjects. For the auditory oddball experiment, there were 34 healthy, right-handed, male volunteers in the age group from 18 to 61. IRB-approved informed consent at the University of New Mexico was obtained from all the participants. Each participant was presented with a practice block of 10 trials prior to the actual scan to ensure understanding of the instructions. Omission errors

included any missed target tones or any response with a latency of greater than the reaction time from target stimulus.

Paradigms—The first paradigm was a motor tapping (MT) paradigm; a block design with periods of 30 s off and 30 s on. The subjects tapped their right-hand fingers during the on period and rest during the off cycle. There were five and a half cycles, starting with off and ending with the off period. For each subject, 165 whole head fMRI images were collected for each subject. The total experiment time was 5 min.

The second paradigm was a three-stimulus auditory oddball (AOD); two runs of 244 auditory stimuli consisting of standard, target, and novel stimuli were presented to the subject. The standard stimulus was a 1000-Hz tone, the target stimulus was a 1500-Hz tone, and the novel stimuli consisted of non-repeating random digital noises. The target and novel stimuli each was presented at a probability of 0.10, and the standard stimuli with a probability of 0.80. The stimulus duration was 200 ms with a 2000-ms stimulus onset asynchrony (SOA). Both the target and novel stimuli were always followed by at least 3 standard stimuli. Steps were taken to make sure that all participants could hear the stimuli and discriminate them from the background scanner noise. Subjects were instructed to respond to the target tone with their right index finger and not to respond to the standard tones or the novel stimuli.

fMRI experimental procedure

All MT imaging was performed on a 3-T Siemens TIM system with a 12-channel radio frequency (RF) coil. The fMRI experiment used a gradient-echo EPI sequence modified so that it stored real and imaginary data separately. The following parameters were used: field of view (FOV)=24 cm, slice thickness=3.5 mm, slice gap=1 mm, number of slices=32, matrix size=64×64, TE=29 ms, TR=2 s, flip angle 70 deg. We collected 15 whole head fMRI images during each ‘ON’ or ‘OFF’ period. The first 6 images were discarded to allow for T1 effects to stabilize.

All AOD imaging was performed on a 1.5-T Siemens Avanto TIM system with a 12-channel RF coil. Conventional spin-echo T1-weighted sagittal localizers were acquired for use in prescribing the functional image volumes. Echo planar images were collected with a gradient-echo sequence, modified so that it stored real and imaginary data separately, with the following parameters: FOV=24 cm, slice thickness=4.0 mm, slice gap=1 mm, number of slices=27, matrix size=64×64, TE=39 ms, TR=2 s, flip angle 75 deg. The participant's head was firmly secured using a custom head holder. The two stimulus runs consisted of 189 time points each. The first 6 images of each run were discarded to allow for T1 effects to stabilize.

Preprocessing

The magnitude and phase images were written out as 4D NIfTI (Neuroimaging Informatics Technology Initiative) files using a custom reconstruction program on the scanner. Preprocessing of the data was done using the SPM5 software package (http://www.fil.ion.ucl.ac.uk/spm/software/spm5/). Magnitude data were co-registered using INRIAlign (Freire and Mangin, 2001; Freire et al., 2002) to compensate for movement in the fMRI time series images. Images were then spatially normalized into the standard Montreal Neurological Institute (MNI) space. Following spatial normalization, the data (originally acquired at 3.75×3.75×4.5 mm^3) were slightly sub-sampled to 3×3×3 mm^3, resulting in 53×63×46 voxels. Motion correction and spatial normalization parameters were computed from the magnitude data and then applied to the phase data. The magnitude and phase data were both spatially smoothed with a 10×10×10-mm^3 full-width at half-maximum Gaussian kernel. Phase and magnitude data were masked to exclude non-brain voxels.

Whole brain analysis

A standard general linear model (GLM) analysis on each individual subject was performed using the SPM5 software. Activation maps were computed for magnitude and phase data separately using the multiple regression frame work within SPM5 in which regressors are created from the stimulus onset times and convolved with a standard hemodynamic response function in SPM (a combination of two gamma functions which has a peak at 6 s).

For motor tapping, one regressor was used to model the on condition. To compute the group maps, a second level random effects analysis was performed using the activation maps (regression parameters) from each individual subject and entering them into a voxelwise one-sample *t*-test (Mumford and Nichols, 2009). The highest magnitude change was observed in the motor cortex.

For auditory oddball, three regressors modeling the target, novel, and standard stimuli were used for each run. A contrast for the average of the novel stimuli across the two runs was computed. Novel stimuli were used since they are known to robustly activate bilateral temporal lobe regions. A second level, random effects analysis was then performed by submitted the novel contrast images to a voxelwise one-sample *t*-test.

ROI analysis: time locked averaging

Next, in order to evaluate the time courses within specific regions an ROI analysis was performed. A band-pass digital Butterworth filter of order 8 with pass band (0.05 and 0.7 Hz) was applied to the time courses to attenuate the effects of low frequency scanner drift and high frequency noise.

For motor tapping, a mask was created from the software package wfu_pickatlas (http://fmri.wfubmc.edu/cms/software#PickAtlas) selecting Brodmann areas 3 and 4 and dilating by one voxel in *x*, *y*, and *z*. Time locked averaging (TLA) for each subject was performed for the 10% of voxels with the largest *t*-values within each region of interest. The mean TLA and the standard error across the subjects were calculated on both magnitude and phase data. For auditory oddball, the region of interest was the temporal lobe, also created via wfu_pickatlas in the same manner. All 35 subjects were analyzed and mean values across the subjects for both magnitude and phase were calculated. TLA plots along with the standard error were plotted.

Results

Fig. 1 shows the magnitude change and phase change of the results for motor tapping and auditory oddball. As expected the highest magnitude change for motor tapping was observed in the left motor cortex and for the auditory oddball highest change was in bilateral temporal lobe. Similarly, maximal phase changes were also observed in motor cortex for MT and in temporal lobe for AOD. The images in the top-right and bottom-right panels of Fig. 1 are the RGB (R—red, G—greed, B—blue) color maps for MT and AOD similar to the display provided in (Rowe, 2005a). The areas in red are where only significant magnitude signal changes were observed, the ones in green are for significant phase-only signal changes and the areas in blue are where both significant magnitude and significant phase signal changes were observed. The resulting signal change changes for phase and magnitude data for both motor tapping and AOD were cluster thresholded to correct for multiple comparisons at $p<0.05$ family-wise error (FWE).

The time locked averaging results for motor tapping and the spatial locations of the voxels are presented in Fig. 2. We show TLA results for voxels which had maximum magnitude response (Fig. 2.1a), the corresponding anatomical map (Fig. 2.1b) displaying the voxels with the

maximum magnitude response considered for the analysis, TLA results for voxels which had maximum positive (Fig. 2.2) and negative (Fig. 2.3) phase response, and TLA results for voxels significant positive (Fig. 2.4) and negative (Fig. 2.5) phase response with insignificant magnitude response. The dotted lines are mean response±standard error. Thus, as has been shown previously (Feng et al., 2009), the phase response can be positive and negative in different spatial locations, these locations of maximum phase response do not coincide with those of maximum magnitude response, and we also observed statistically significant phase response in regions expected to be activated by the task but where the magnitude response is not significant.

Fig. 3 shows the detrended and band-pass filtered time courses for the magnitude and phase for the block-design motor tapping. Fig. 3a shows the observed magnitude time course in cyan and the reference signal in yellow. Fig. 3b and c show plots corresponding to positive and negative phase.

Fig. 4 is similar to Fig. 2 and shows the time locked averaging and the corresponding anatomical maps for auditory oddball novel stimuli. We focused only upon the novel stimuli in this study since novel stimuli are a robust activator of temporal lobe.

We also incorporated an additional step to remove small clusters. After thresholding, the group results were processed with a contiguity filter to remove voxels with less than 150 connected voxels (Hofer et al., 2003). Fig. 5 represents the phase activation maps of a single subject performing the motor tapping task.

A quantitative analysis of the degree to which the voxels are active in the regions expected to be active by the task is presented in Table 1. The table shows the values for the maximum percentage signal change averaged across subjects for magnitude and phase data as well as the standard deviation across the subjects and the ratio of mean/SD. Though the percentage signal change is small in the phase data compared to that in the magnitude the standard deviation is also lower for the phase data. The ratio of the % signal change to the standard deviation in the data is in the same range as that of the magnitude data resulting in similar significance values for magnitude and phase data.

Discussion

We have evaluated the correspondence between task-related changes in magnitude and phase data with the expectation that the changes also occur in phase. The goal was to investigate the phase changes observed in both block and event-related design studies and specifically to determine if these changes were in regions expected to be involved in the tasks. The data were analyzed using two different approaches to illustrate that the signal changes in phase were consistent with the signal changes in magnitude in both the experimental paradigms.

The signal changes were studied using different processing methods including region of interest analysis (ROI) and whole brain analysis. The ROI analysis of motor tapping (MT) data and auditory oddball (AOD) showed signal changes (in both magnitude and phase data separately) as expected. The positive and negative phase signal changes are present for both the MT and AOD tasks. In the ROI analysis, we study the signal changes in regions of interest that were expected to show changes associated with the MT and AOD tasks.

For the MT task, the voxel with highest task-related magnitude change showed a small phase signal consistent with theoretical and empirical results presented in (Feng et al., 2009). The voxel with maximum positive/negative phase showed statistically significant magnitude signal change suggesting that the phase signal changes are concurrent with magnitude signal change. The phase changes are present in both block and event-related design at a group level. The

standard error plots confer the fact that the phase showed consistent signal change across the subjects in the group (Fig. 2, Fig. 4, and Fig. 5). Though the percentage signal change in the phase data is low compared to that of the magnitude, the standard deviation across subjects is also smaller. Some of the voxels in the regions expected to be activated showed significant task-related phase changes with no observable magnitude changes, which suggests that phase data may hold useful information. However, further studies should be conducted to determine the cause of these effects since it is known that phase signals can arise from both large vessels as well as randomly oriented micro-vascular regions (Feng et al., 2009; Zhao et al., 2007). For whole brain group studies done at relatively low resolution, both of these causes for phase signal change may provide a useful amplification of the BOLD effect at the cost of some loss of spatial specificity.

The second level analysis, on the *t*-maps of individual subjects, was performed for whole brain analysis at the group level. The maps presented in the results show that there are quite a few voxels that are activated for both phase and magnitude data. The color maps in Fig. 1 show voxels with only phase change, only magnitude change, or both phase and magnitude signal changes. The maps emphasize the fact that the active voxels occurred in regions that are expected to be activated by the task. Table 2 gives a quantitative comparison of the number of voxels that were active in magnitude only, phase only and in both magnitude and phase. In both AOD and MT, there are a significant number of voxels (in the regions expected to be activated by the task) that showed statistically high phase signal change with insignificant magnitude signal change. The ROI analysis results reconfirm this fact. Our study demonstrates that significant phase signal changes for group studies can be found for both block and event-related design. We incorporated several preprocessing steps including phase correction, masking, temporal filtering, and cluster removal. As phase data become more widely used, it will be important to optimize the preprocessing steps as has been done in many papers for magnitude fMRI data. We performed a voxelwise analysis of the data. Table 3 shows the amplitude of signal change peaks for MT data for magnitude and phase separately and their corresponding MNI coordinates. Table 4 represents the amplitude of signal change peaks for AOD data and the corresponding MNI coordinates.

The color activation maps in Fig. 1 show the correspondence between the magnitude and phase responses. The regions of interest in each of these maps are labeled such that red shows magnitude-only areas, green shows phase only, and the areas for magnitude and phase are shown by blue. Table 5 and Table 6 give us the corresponding peak signal changes and their MNI coordinates for motor tapping and auditory oddball tasks. Tapping movement mainly activates regions in the motor cortex; hence for the motor tapping paradigm, it is expected to see peaks in precentral gyrus. All the sub-sessions in Table 5 show activation/peaks in this area. From the auditory oddball paradigm, it is a known fact the novels mainly activate the temporal lobes; Table 6 shows peak signal changes in the superior temporal gyrus in all the sub-sessions. The results are encouraging and corroborate with patterns observed in the ROI analysis. The presence of these areas in phase-only activation maps (without any magnitude signal change) suggests that using the phase date in fMRI may provide useful information beyond the magnitude data.

Conclusion

Separate analyses of phase and magnitude fMRI data at a group level for two different paradigms was analyzed. The group statistical results show significant phase changes in both block-design and event-related design. The presence of phase activation in the regions expected to be activated by the task suggests that the information in the phase might help increase the ability to isolate the task-related functional changes. To our knowledge, this is the first attempt

to study the phase changes in fMRI BOLD experiments for an event-related design at a group level.

Acknowledgments

This work is supported by NSF grants 0715022 and 0840895.

References

Calhoun VD, Adali T, Pearlson GD, Van Zijl PCM, Pekar JJ. Independent component analysis of fMRI data in the complex domain. Magn. Reson. Med 2002;48(1):180–192. [PubMed: 12111945]

Deshmukh AV, Shivhare V, Gadre VM, Patkar DP, Pungavkar SSS. A phase based method for investigating the functional connectivity in the fMRI data. 2004 Dec 20–22;:272–277.

Feng Z, Caprihan A, Blagoev K, Calhoun VD. Biophysical modeling of phase changes in BOLD fMRI. NeuroImage 2009;47:540–548. [PubMed: 19426815]

Freire L, Mangin JF. Motion correction algorithms may create spurious brain activations in the absence of subject motion. NeuroImage 2001;14(3):709–722. [PubMed: 11506543]

Freire L, Roche A, Mangin JF. What is the best similarity measure for motion correction in fMRI time series? Med. Imaging IEEE Trans 2002;21(5):470–484.

Hofer A, Weiss EM, Golaszewski SM, Siedentopf CM, Brinkhoff C, Kremser C, Felber S, Fleischhacker WW. An fMRI study of episodic encoding and recognition of words in patients with schizophrenia in remission. Am. J. Psychiatry 2003;160(5):911–918. [PubMed: 12727695]

Hoogenraad FGC, Reichenbach JR, Haacke EM, Lai S, Kuppusamy K, Sprenger M. In vivo measurement of changes in venous blood-oxygenation with high resolution functional MRI at 0.95 Tesla by measuring changes in susceptibility and velocity. Magn. Reson. Med 1998;39(1):97–107. [PubMed: 9438443]

Hoogenraad FGC, Pouwels PJW, Hofman MBM, Reichenbach JR, Sprenger M, Haacke EM. Quantitative differentiation between BOLD models in fMRI. Magn. Reson. Med 2001;45(2):233–246. [PubMed: 11180431]

Laird AR, Rogers BP, Carew JD, Arfanakis K, Moritz CH, Meyerand ME. Characterizing instantaneous phase relationships in whole-brain fMRI activation data. Hum. Brain Mapp 2002;16(2):71–80. [PubMed: 11954057]

Lee J, Shahram M, Schwartzman A, Pauly JM. Complex data analysis in high-resolution SSFP fMRI. Magn. Reson. Med 2007;57(5):905–917. [PubMed: 17457883]

Menon RS. Postacquisition suppression of large-vessel BOLD signals in high-resolution fMRI. Magn. Reson. Med 2002;47(1):1–9. [PubMed: 11754436]

Miller, KL.; Hargreaves, BA.; Lee, J.; Ress, D.; deCharms, RC.; Pauly, JM. Functional brain imaging with BOSS FMRI. Engineering in Medicine and Biology Society, 2004; IEMBS '04. 26th Annual International Conference of the IEEE; 2004 Sept 1–5. p. 5234-5237.

Mumford JA, Nichols T. Simple group fMRI modeling and inference. NeuroImage 2009;47(4):1469–1475. [PubMed: 19463958]

Nencka AS, Rowe DB. Reducing the unwanted draining vein BOLD contribution in fMRI with statistical post-processing methods. NeuroImage 2007;(37):177–188. [PubMed: 17560130]

Petridou N, Schäfer A, Gowland P, Bowtell R. Phase vs. magnitude information in functional magnetic resonance imaging time series: toward understanding the noise. Magn. Reson. Imaging 2009;27(8):1046–1057. (Oct). [PubMed: 19369024]

Rowe DB. Modeling both the magnitude and phase of complex-valued fMRI data. NeuroImage 2005a;25(4):1310–1324. [PubMed: 15850748]

Rowe DB. Parameter estimation in the magnitude-only and complex-valued fMRI data models. NeuroImage 2005b;25(4):1124–1132. [PubMed: 15850730]

Rowe DB, Logan RB. A complex way to compute fMRI activation. NeuroImage 2004;23(3):1078–1092. [PubMed: 15528108]

Rowe DB, Logan RB. Complex fMRI analysis with unrestricted phase is equivalent to a magnitude-only model. NeuroImage 2005;24(2):603–606. [PubMed: 15627605]

Tomasi DG, Caparelli EC. Macrovascular contribution in activation patterns of working memory. Epub 2007;27(1):33–42.

Weaver JB. Applications of monotonic noise reduction algorithms in fMRI, phase estimation, and contrast enhancement. Int. J. Imaging Syst. Technol 1999;10(2):177–185.

Zhao F, Jin T, Wang P, Hu X, Kim SG. Sources of phase changes in BOLD and CBV-weighted fMRI. Magn. Reson. Med 2007;57(3):520–527. [PubMed: 17326174]

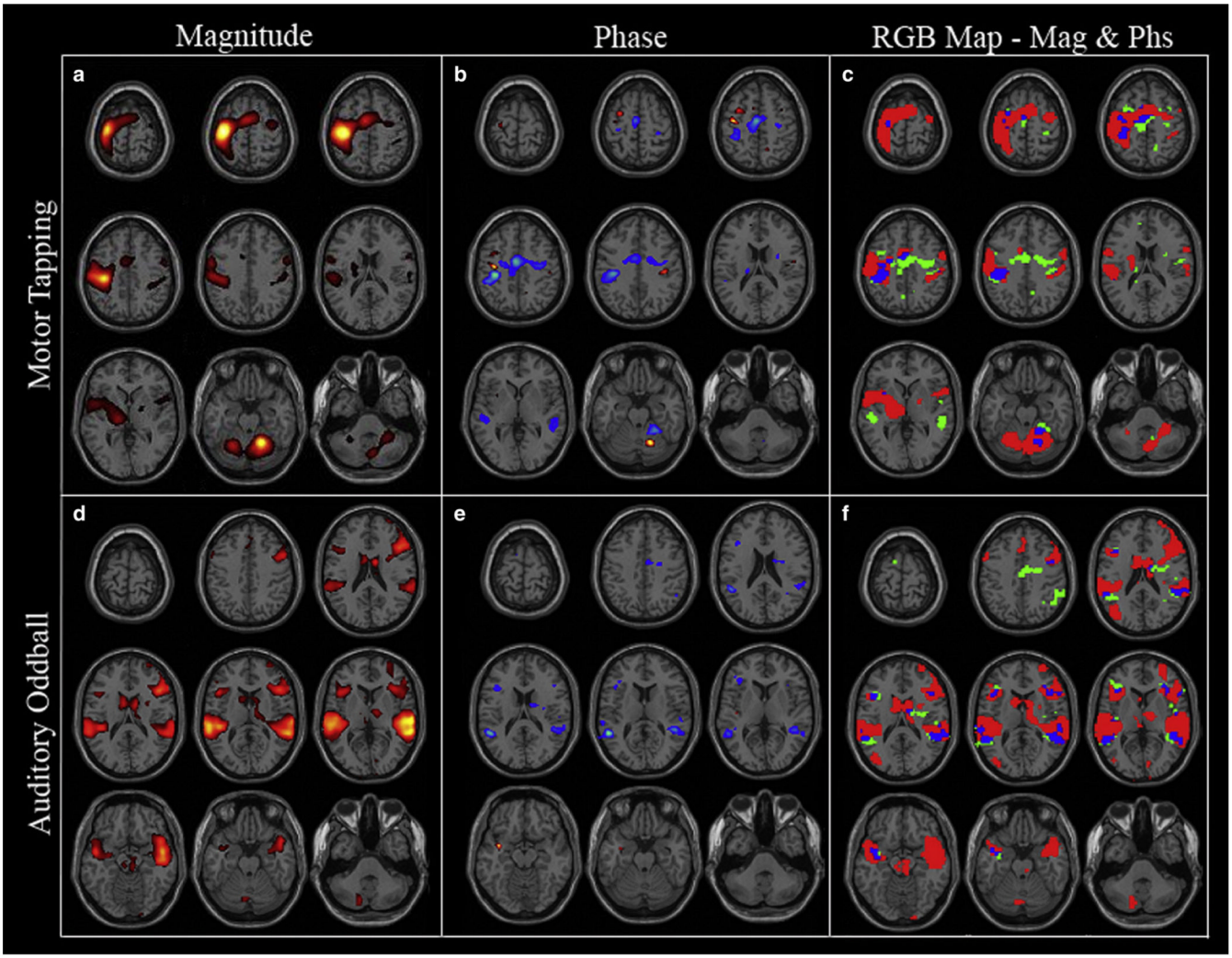

Fig. 1.

Group whole brain analysis results for motor tapping and auditory oddball. (a) Group magnitude results for motor tapping, (b) group phase results for motor tapping, (c) color maps for motor tapping – red, magnitude only; green, phase only; blue, magnitude and phase – (d) group magnitude results for auditory oddball, (e) group phase results for auditory oddball, (f) color maps for auditory oddball–red, magnitude only; green, phase only; blue, magnitude and phase.

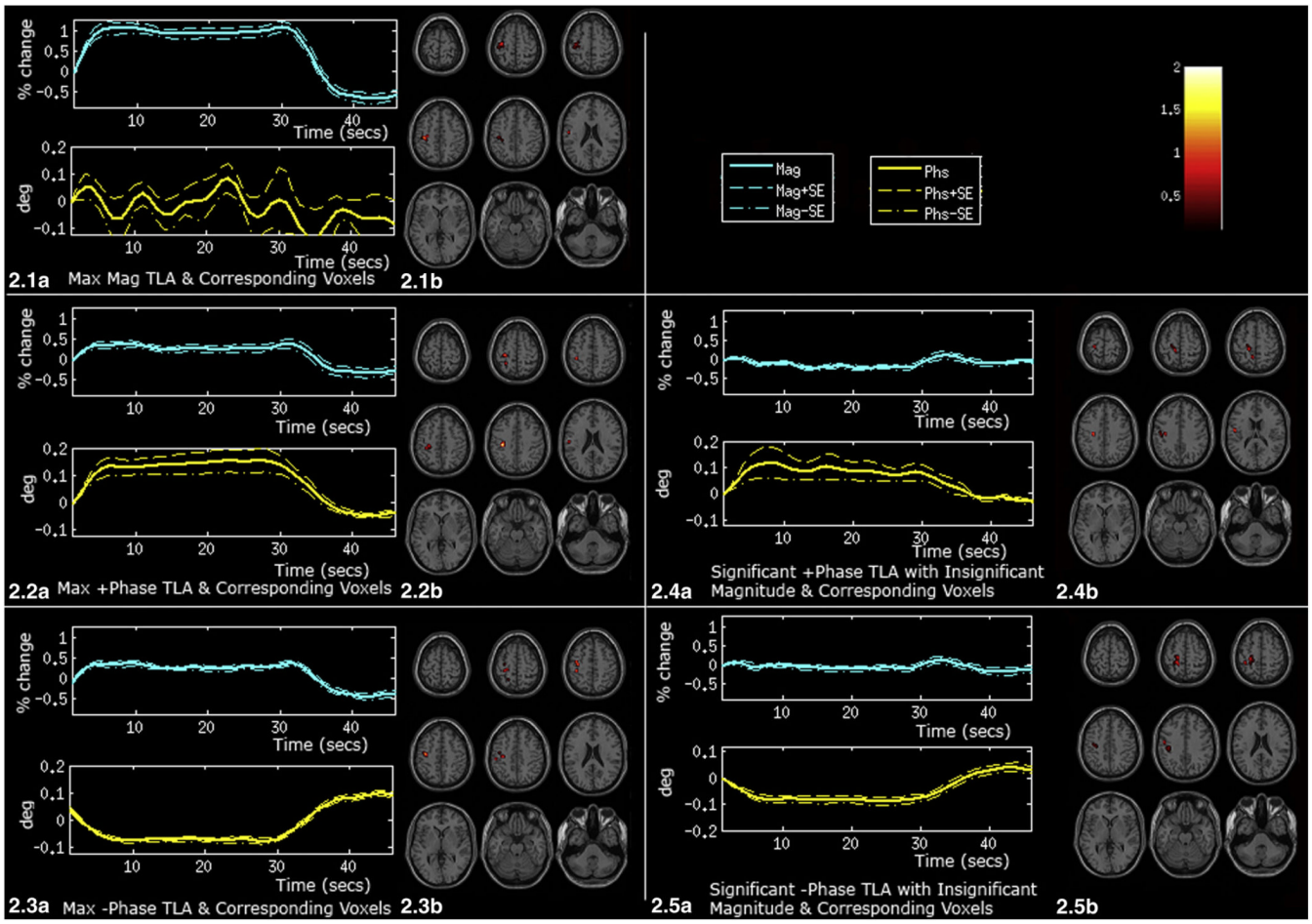

Fig. 2.

Group ROI analysis results for motor tapping and the corresponding voxel indices. (a) TLA at voxel with maximum magnitude and voxel indices maps, (b) TLA at voxel with maximum positive phase and voxel indices maps, (c) TLA at voxel with maximum negative phase and voxel indices maps, (d) TLA at voxel with significant positive phase activation and insignificant magnitude activation and the corresponding voxel indices maps, (e) TLA at voxel with significant negative phase activation and insignificant magnitude activation and the corresponding voxel indices maps.

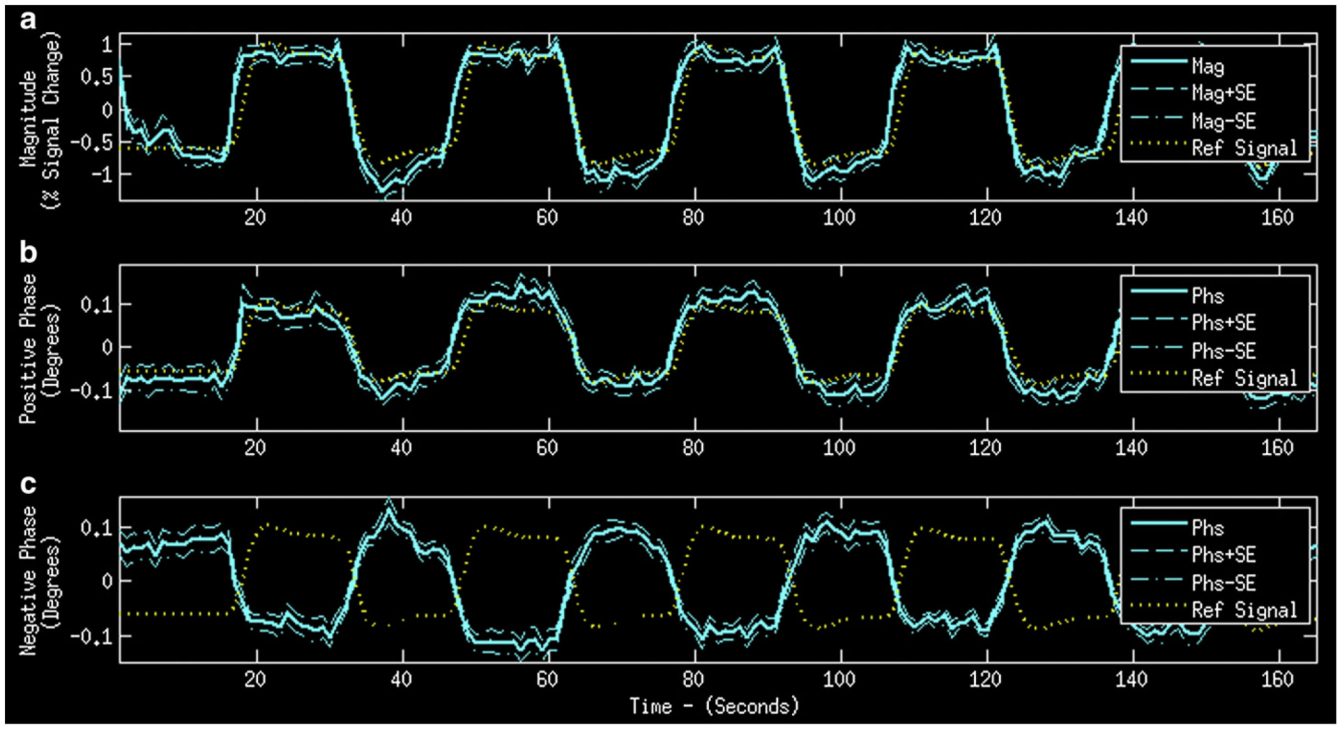

Fig. 3.
Magnitude and phase fMRI time courses for MT.

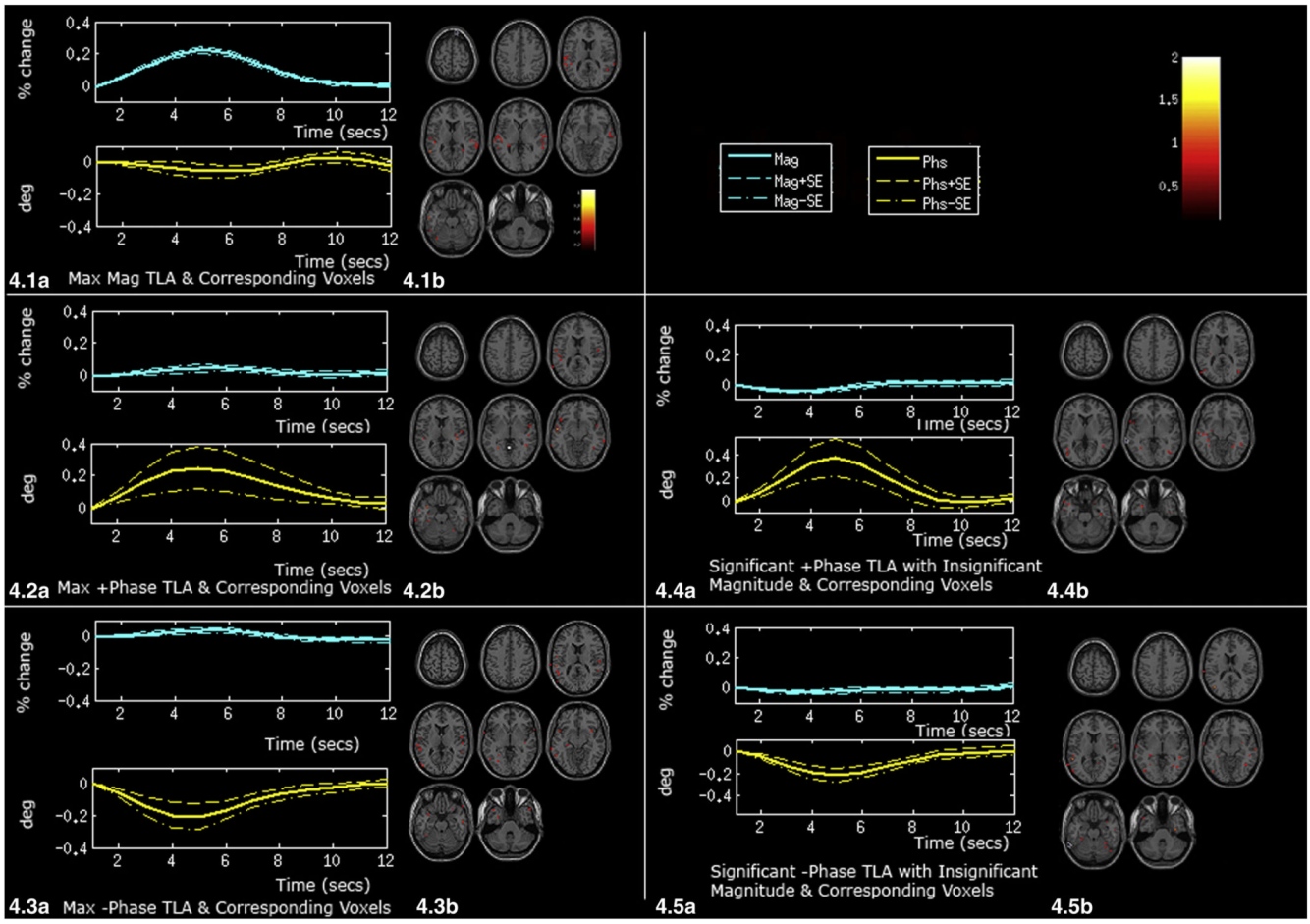

Fig. 4.

Group RIO analysis results for auditory oddball and the corresponding voxel indices. (a) TLA at voxel with maximum magnitude and voxel indices maps, (b) TLA at voxel with maximum positive phase and voxel indices maps, (c) TLA at voxel with maximum negative phase and voxel indices maps, (d) TLA at voxel with significant positive phase activation and insignificant magnitude activation and the corresponding voxel indices maps, (e) TLA at voxel with significant negative phase activation and insignificant magnitude activation and the corresponding voxel indices maps.

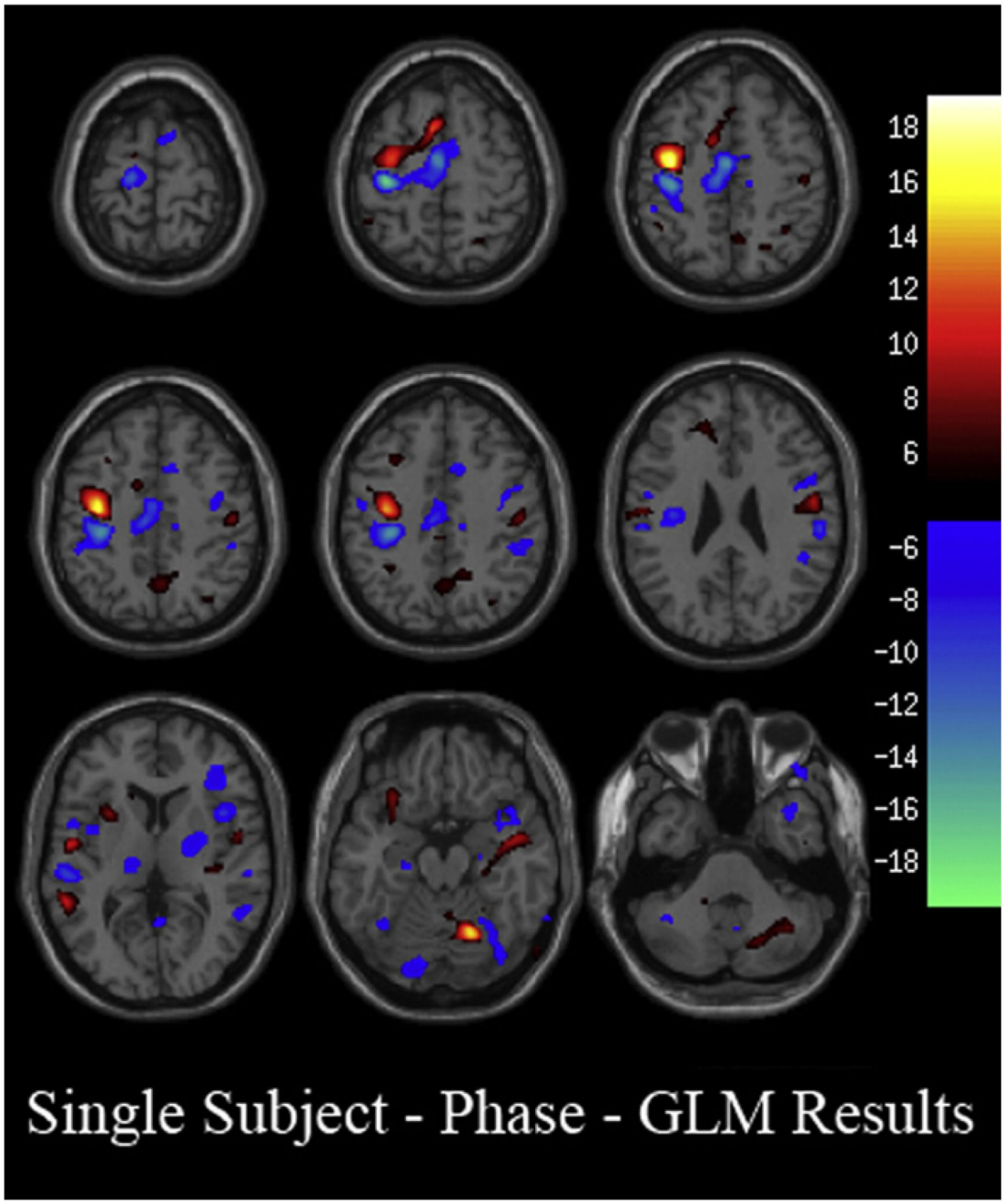

Fig. 5.
Phase map from a representative subject showing a similar pattern as found in the group maps.

Table 1

Quantitative analysis results for magnitude and phase data.

	%Signal change –magnitude	SD magnitude	Ratio %signal change of magnitude to magnitude SD	%Signal change –phase	SD phase	Ratio %signal change of phase to phase SD
Motor tapping						
Max magnitude	1.0959	0.6029	1.81771438	0.066	0.2192	0.30109489
Max +ve phase	0.3691	0.3421	1.07892429	0.09	0.0656	1.37195122
Max −ve phase	0.3608	0.4507	0.8005325	0.0847	0.0238	3.55882353
Auditory oddball						
Max magnitude	0.2226	0.1207	1.84424192	0.0169	0.1096	0.15419708
Max +ve phase	0.0402	0.0391	1.02813299	0.137	0.087	1.57471264
Max −ve phase	0.038	0.0376	1.0106383	0.1141	0.072	1.58472222

Table 2

Voxels counts for auditory oddball and motor tapping.

	Voxel count
Auditory oddball	
Magnitude and phase	872
Magnitude only	8251
Phase only	952
Motor tapping	
Magnitude and phase	912
Magnitude only	6421
Phase only	1642

Table 3

MNI table for motor tapping.

	Area	Brodmann area	L/R volume	L/R random effects: max *T* (*x*, *y*, *z*)
Magnitude				
	Precentral gyrus	4, 6, 44	4.8/20.6	4.4 (−56,5,36)/14.9 (39,−15,56)
	Postcentral gyrus	3, 4, 2, 40, 1, 5, 43, 7	3.6/15.8	3.3 (−50,−21,37)/13.9 (42,−18,53)
	Cerebellum		29.3/12.9	13.8 (−21,−53,−18)/7.3 (24,−56,−17)
	Middle frontal gyrus	6, 9, 8	2.7/6.3	4.4 (−56,2,39)/11.6 (30,−9,61)
	Superior frontal gyrus	6	2.8/3.8	5.7 (0,6,52)/11.5 (33,−8,64)
	Medial frontal gyrus	6, 32	3.2/4.7	6.4 (0,3,52)/7.4 (6,0,53)
	Fusiform gyrus	19, 37	0.9/NA	6.7 (−21,−56,−10)/NA
	Inferior parietal lobule	40	0.6/5.6	3.1 (−36,−30,40)/6.7 (45,−30,46)
	Cingulate gyrus	24, 31, 32	1.2/2.5	5.3 (0,2,47)/6.3 (6,−1,47)
	Culmen of vermis		0.3/0.1	6.3 (−3,−65,−9)/4.0 (3,−65,−9)
	Thalamus		NA/4.9	NA/5.8 (15,−17,4)
	Inferior frontal gyrus	9, 44, 45, 47	2.1/2.3	4.3 (−56,7,33)/5.5 (59,7,27)
	Lingual gyrus	18, 19	1.2/0.1	5.0 (−18,−70,−9)/2.7 (3,−76,−6)
	Lentiform nucleus		0.7/5.4	2.8 (−21,−3,−2)/4.9 (21,−6,−5)
	Insula	13, 40	0.5/5.7	2.9 (−45,9,−3)/4.8 (48,3,3)
	Superior temporal gyrus	22, 41, 38, 42	1.5/4.1	3.1 (−48,9,−3)/4.6 (50,3,0)
	Paracentral lobule		NA/0.1	NA/3.8 (6,−9,47)
	Superior parietal lobule	7, 5	NA/1.2	NA/3.8 (30,−47,60)
	Precuneus	7	NA/0.1	NA/3.3 (30,−47,52)
	Parahippocampal gyrus		NA/0.2	NA/3.0 (27,−4,−12)
	Transverse Temporal gyrus	41, 42	NA/0.6	NA/3.0 (56,−17,12)
	Lateral ventricle		NA/0.1	NA/2.6 (24,−15,−7)
Phase positive				
	Precentral gyrus	6, 43, 13, 9	1.3/1.9	4.0 (−39,−19,34)/4.8 (36,−12,45)
	Middle frontal gyrus	6	0.2/2.1	2.8 (−33,6,52)/4.7 (33,−12,45)
	Cerebellum		2.5/NA	4.7 (−18,−62,−15)/NA
	Postcentral gyrus	3, 2	1.1/NA	3.7 (−39,−16,31)/NA
	Precuneus	7,31	0.6/0.2	3.2 (−15,−50,49)/2.7 (3,−59,44)
	Cingulate gyrus	31	0.2/0.1	3.2 (−15,−42,27)/2.8 (12,−42,27)
	Superior temporal gyrus	22	0.1/0.1	2.6 (−50,−3,3)/2.9 (50,−11,9)
	Medial frontal gyrus	6	NA/0.2	NA/2.8 (9,8,52)
	Superior frontal gyrus	6	NA/0.2	NA/2.8 (6,8,52)
	Insula		0.1/0.2	2.6 (−45,−11,17)/2.7 (45,6,−3)
Phase negative				
	Postcentral gyrus	3, 2, 40, 5	0.9/5.9	2.2 (−50,−30,35)/7.9 (33,−24,43)
	Cingulate gyrus	24, 31, 32, 23	6.9/8.9	6.9 (0,−7,45)/7.3 (3,−7,45)
	Paracentral lobule	31, 6	0.4/1.5	6.5 (0,−9,47)/7.1 (3,−9,47)
	Medial frontal gyrus	6, 10, 32	2.1/4.7	5.8 (0,−9,50)/6.6 (3,−9,50)

	Area	Brodmann area	L/R volume	L/R random effects: max *T* (*x*, *y*, *z*)
	Precentral gyrus	4, 6	5.9/2.8	4.3 (−36,−10,42)/6.2 (39,−21,37)
	Cerebellum		6.1/2.6	5.8 (−27,−44,−15)/2.8 (24,−42,−21)
	Parahippocampal gyrus	37, 19, 36, 28, 30	1.9/1.4	5.5 (−21,−47,−10)/3.7 (36,−33,−11)
	Inferior parietal lobule	40	2.8/6.7	2.3 (−42,−36,46)/5.5 (45,−25,29)
	Fusiform gyrus	37, 19, 20	2.5/1.9	4.3 (−21,−53,−7)/3.6 (36,−36,−11)
	Middle temporal gyrus	22, 21, 37, 39	7.9/3.7	4.0 (−56,−35,−1)/2.6 (48,−32,2)
	Middle frontal gyrus	6, 11, 9	1.3/0.3	4.0 (−30,−12,45)/4.0 (24,−7,45)
	Superior temporal gyrus	41, 22, 42, 21, 39, 13	7.1/8.4	4.0 (−53,−34,10)/3.9 (45,−34,13)
	Transverse temporal gyrus	41, 42	0.4/0.8	2.6 (−50,−26,10)/3.7 (45,−31,13)
	Lingual gyrus	18, 17, 19	2.9/2.5	3.0 (−21,−87,−1)/3.5 (18,−88,−3)
	Lateral ventricle		0.5/1.2	2.6 (−36,−35,−6)/3.2 (36,−32,−8)
	Cerebellum		4.6/0.7	3.2 (−18,−57,−35)/2.5 (21,−56,−10)
	Basal ganglia		1.6/0.7	3.0 (−24,−15,−2)/2.9 (30,−18,−4)
	Thalamus		0.1/1.0	1.9 (−15,−15,1)/2.9 (15,−17,17)
	Insula	13, 45	2.3/2.1	2.7 (−30,1,17)/2.8 (50,−22,20)
	Inferior occipital gyrus	18, 19	0.6/0.1	2.7 (−30,−82,−3)/2.0 (21,−88,−8)
	Supramarginal gyrus	40	0.5/0.2	2.2 (−39,−42,33)/2.6 (45,−36,35)
	Anterior cingulate	10, 33, 32, 24	1.8/0.7	2.5 (−12,29,−6)/2.5 (12,13,24)
	Middle occipital gyrus	18	0.4/0.1	2.5 (−27,−84,2)/1.8 (36,−76,1)
	Inferior frontal gyrus	47, 13, 9, 45, 6	1.2/0.4	2.5 (−21,32,−7)/1.8 (48,1,19)
	Cuneus	17, 18	0.6/0.2	2.3 (−6,−84,7)/2.1 (15,−93,0)
	Precuneus	31, 23, 7	0.8/NA	2.1 (−12,−63,28)/NA
	Inferior temporal gyrus	21, 37	0.2/NA	1.9 (−56,−12,−15)/NA
	Posterior cingulate	31	0.1/NA	1.7 (−3,−60,22)/NA

Table 4

MNI table for auditory oddball.

	Area	Brodmann area	L/R volume	L/R random effects, Max *T* (*x*, *y*, *z*)
Magnitude	Superior temporal gyrus	22, 21, 41, 38, 42, 13, 39	27.9/21.7	10.7 (−59,−20,1)/8.2 (59,−29,10)
	Middle frontal gyrus	46, 6, 9, 8, 10	18.8/5.8	6.9 (−45,16,27)/5.4 (39,16,27)
	Inferior frontal gyrus	9, 45, 46, 47, 13, 44, 10	17.3/6.8	7.2 (−45,24,13)/5.5 (39,20,−1)
	Middle temporal gyrus	21, 22, 38, 39	14.8/6.8	9.8 (−48,−21,−4)/7.2 (50,−18,−4)
	Insula	13, 22, 47, 41, 40, 45	6.2/8.1	7.3 (−42,−23,1)/7.3 (45,−15,−2)
	Superior frontal gyrus	6, 8, 10, 9	6.0/1.0	5.3 (−6,14,49)/4.6 (3,17,49)
	Lingual gyrus	17, 18	4.4/1.7	5.6 (−18,−93,−3)/4.7 (3,−87,−1)
	Thalamus		3.2/1.1	4.6 (−12,−9,3)/4.3 (6,−9,0)
	Inferior parietal lobule	40	2.5/1.9	4.9 (−62,−37,24)/4.3 (45,−34,24)
	Cuneus	17, 18	2.3/1.3	5.8 (−15,−93,0)/4.4 (3,−93,0)
	Medial frontal gyrus	8, 6, 32	2.2/0.9	5.4 (−6,20,46)/4.4 (3,17,46)
	Transverse temporal gyrus	41, 42	1.6/1.8	6.6 (−50,−26,10)/7.5 (45,−31,13)
	Caudate		1.4/1.5	5.6 (−12,1,19)/5.0 (9,4,16)
	Postcentral gyrus	40, 43	1.4/1.7	6.1 (−65,−23,15)/6.6 (56,−25,15)
	Cingulate gyrus	32, 23	1.3/0.8	4.2 (−12,−2,28)/4.1 (3,−22,26)
	Precentral gyrus	44, 6, 9, 13	1.3/0.6	5.0 (−53,5,44)/5.3 (45,18,7)
	Cerebellum		0.5/6.2	3.8 (0,−74,−14)/5.4 (15,−80,−24)
	Parahippocampal gyrus		0.5/0.6	4.5 (−33,−4,−17)/4.6 (27,−9,−12)
	Supramarginal gyrus	40	0.5/NA	3.8 (−62,−46,22)/NA
	Inferior occipital gyrus	17	0.1/NA	3.1 (−21,−97,−8)/NA
	Inferior temporal gyrus	21	0.1/NA	3.6 (−56,−7,−15)/NA
	Posterior cingulate	23	NA/0.1	NA/3.5 (3,−28,24)
Positive phase	Superior temporal gyrus	22	NA/0.7	NA/3.7 (36,−1,−15)
	Insula	13	NA/1.0	NA/3.5 (39,−17,4)
	Parahippocampal gyrus		NA/0.2	NA/3.3 (33,−4,−15)
	Middle temporal gyrus	21	NA/0.1	NA/2.3 (42,4,−28)
Negative phase	Inferior parietal lobule	40	3.7/0.7	3.6 (−53,−42,24)/5.8 (48,−46,22)
	Middle temporal gyrus	21, 39, 22, 37	1.2/1.4	4.4 (−48,−41,2)/4.7 (53,−46,8)
	Insula	13, 47	2.5/0.4	4.3 (−45,−40,19)/3.4 (39,21,13)
	Supramarginal gyrus	40	1.8/0.2	4.3 (−50,−45,30)/4.1 (50,−48,22)
	Inferior frontal gyrus	45, 6, 9, 47, 13, 46	2.6/1.9	4.0 (−39,2,30)/4.0 (42,21,13)
	Cingulate gyrus	24	2.2/0.2	3.8 (−9,−7,39)/2.5 (3,−13,37)
	Precentral gyrus	6, 9	1.1/NA	3.6 (−42,1,28)/NA
	Caudate		0.2/NA	3.3 (−12,−2,17)/NA
	Postcentral gyrus	40	0.6/NA	3.1 (−53,−23,15)/NA
	Middle frontal gyrus	9, 11, 46, 47	0.2/0.5	2.2 (−48,5,36)/3.0 (36,41,−5)
	Superior frontal gyrus	6	NA/0.5	NA/3.0 (9,6,63)

Area	Brodmann area	L/R volume	L/R random effects, Max *T* (*x*, *y*, *z*)
Inferior temporal gyrus	37, 21	NA/0.1	NA/2.7 (65,−53,−5)
Medial frontal gyrus	6	0.6/0.2	2.6 (−12,3,58)/2.6 (3,3,52)
Angular gyrus		0.1/NA	2.3 (−36,−54,30)/NA

Table 5

MNI table for RGB maps of motor tapping.

	Area	Brodmann area	L/R volume	L/R random effects, max *T* (*x*, *y*, *z*)
Magnitude (magnitude and phase)	Precentral gyrus	4, 6	0.0/3.3	2.6 (−45,−21,37)/14.1 (36,−12,56)
	Postcentral gyrus	3, 2, 40	0.1/3.9	3.1 (−48,−21,40)/13.0 (36,−21,45)
	Cerebellum		5.1/NA	12.8 (−21,−56,−17)/NA
	Middle frontal gyrus	6	NA/0.9	NA/10.1 (27,−11,61)
	Medial frontal gyrus	6	0.4/1.3	5.8 (0,−3,50)/7.1 (6,−3,53)
	Inferior parietal lobule	40	NA/2.8	NA/6.7 (45,−30,46)
	Cingulate gyrus	24, 31	0.5/0.9	5.3 (0,−1,47)/6.3 (6,−1,47)
	Fusiform gyrus	37	0.1/NA	6.3 (−21,−53,−10)/NA
	Superior frontal gyrus	6	NA/0.1	NA/4.3 (6,8,49)
	Insula	13	NA/0.2	NA/4.2 (50,−22,20)
	Paracentral lobule		0.0/0.1	2.8 (0,−9,47)/3.8 (6,−9,47)
	Parahippocampal gyrus		0.0/NA	3.2 (−21,−47,−10)/NA
	Basal ganglia		NA/0.0	NA/3.2 (33,3,−5)
	Thalamus		NA/0.1	NA/3.0 (15,−20,15)
	Transverse temporal gyrus		NA/0.0	NA/2.8 (53,−26,12)
	Superior temporal gyrus	41, 22	NA/0.1	NA/2.6 (50,−31,15)
Magnitude (only magnitude)	Precentral gyrus	4, 6, 44	4.8/17.2	4.4 (−56,5,36)/14.9 (39,−15,56)
	Postcentral gyrus	3, 4, 2, 1, 40, 5, 43, 7	3.5/12.0	3.3 (−50,−21,37)/13.9 (42,−18,53)
	Cerebellum		24.1/12.9	13.8 (−21,−53,−18)/7.3 (24,−56,−20)
	Middle frontal gyrus	6, 9, 8	2.7/5.5	4.4 (−56,2,39)/11.6 (30,−9,61)
	Superior frontal gyrus	6	2.8/3.6	5.7 (0,6,52)/11.5 (33,−8,64)
	Medial frontal gyrus	6, 32	2.8/3.3	6.4 (0,3,52)/7.4 (6,0,53)
	Fusiform gyrus	19, 37	0.8/NA	6.7 (−21,−56,−10)/NA
	Inferior parietal lobule	40	0.6/2.8	3.1 (−36,−30,40)/6.6 (48,−32,57)
	Cingulate gyrus	24, 32	0.7/1.7	5.3 (0,2,47)/6.2 (6,2,47)
	Thalamus		NA/4.9	NA/5.8 (15,−17,4)
	Inferior frontal gyrus	9, 44, 45, 47	2.1/2.3	4.3 (−56,7,33)/5.5 (59,7,27)
	Lingual Gyrus	18, 19	1.2/0.1	5.0 (−18,−70,−9)/2.7 (3,−76,−6)
	Basal ganglia		0.7/5.8	2.8 (−21,−3,−2)/4.9 (21,−6,−5)
	Insula	13, 40	0.5/5.2	2.9 (−45,9,−3)/4.8 (48,3,3)
	Superior temporal gyrus	22, 41, 38, 42	1.5/4.0	3.1 (−48,9,−3)/4.6 (50,3,0)
	Superior parietal lobule	7, 5	NA/1.2	NA/3.8 (30,−47,60)
	Precuneus	7	NA/0.1	NA/3.3 (30,−47,52)
	Transverse temporal gyrus	41, 42	NA/0.6	NA/3.0 (56,−17,12)
	Parahippocampal gyrus		NA/0.2	NA/3.0 (27,−4,−12)
Negative phase (magnitude and phase)	Postcentral gyrus	3, 2, 40	NA/3.9	NA/7.9 (33,−24,43)
	Cingulate gyrus	24, 31	0.5/0.9	6.9 (0,−7,45)/7.3 (3,−7,45)
	Paracentral lobule		0.0/0.1	6.5 (0,−9,47)/7.1 (3,−9,47)

	Area	Brodmann area	L/R volume	L/R random effects, max *T* (*x*, *y*, *z*)
	Medial frontal gyrus	6	0.3/1.3	5.8 (0,−9,50)/6.6 (3,−9,50)
	Precentral gyrus	4	0.1/1.5	3.3 (−36,−13,39)/6.2 (39,−21,37)
	Cerebellum		2.6/NA	5.8 (−27,−44,−15)/NA
	Parahippocampal gyrus		0.0/NA	5.5 (−21,−47,−10)/NA
	Inferior parietal lobule	40	NA/2.8	NA/5.5 (45,−25,29)
	Fusiform gyrus	37	0.1/NA	4.3 (−21,−53,−7)/NA
	Middle frontal gyrus	6	NA/0.1	NA/4.0 (24,−7,45)
	Superior temporal gyrus	41	NA/0.1	NA/3.0 (48,−31,15)
	Insula	13	NA/0.1	NA/2.8 (50,−22,20)
	Thalamus		NA/0.1	NA/2.6 (15,−20,15)
	Basal ganglia		NA/0.0	NA/2.6 (27,−18,−2)
	Transverse temporal gyrus		NA/0.0	NA/2.6 (53,−26,12)
Positive phase (magnitude and phase)	Precentral gyrus	6	0.0/1.8	2.6 (−45,−21,37)/4.8 (36,−12,45)
	Middle frontal gyrus	6	NA/0.8	NA/4.7 (33,−12,45)
	Cerebellum		2.5/NA	4.7 (−18,−62,−15)/NA
	Postcentral gyrus	2, 3	0.1/NA	2.9 (−48,−21,43)/NA
	Medial frontal gyrus	6	0.0/0.1	2.5 (−15,8,52)/2.8 (9,8,52)
	Superior frontal gyrus	6	NA/0.1	NA/2.8 (6,8,52)
	Insula		NA/0.1	NA/2.7 (45,6,−3)
	Superior temporal gyrus	22	NA/0.1	NA/2.7 (53,−11,9)
	Basal ganglia		NA/0.0	NA/2.6 (33,3,−5)
Negative phase (only phase)	Paracentral lobule	31, 6	0.2/0.8	6.3 (0,−9,45)/6.6 (3,−9,45)
	Cingulate gyrus	24, 31	2.3/3.3	5.7 (−3,−7,45)/6.2 (3,−7,42)
	Medial frontal gyrus	6	0.4/1.7	5.3 (0,−12,48)/5.0 (6,−15,48)
	Cerebellum		1.1/0.2	5.2 (−30,−44,−15)/2.8 (24,−42,−21)
	Parahippocampal gyrus	37, 19, 36	0.7/0.4	4.8 (−24,−47,−10)/3.7 (36,−33,−11)
	Inferior parietal lobule	40	NA/1.6	NA/4.5 (36,−25,29)
	Precentral gyrus	6, 4	1.7/NA	4.3 (−36,−10,42)/NA
	Fusiform gyrus	37, 19, 20	0.6/0.3	4.2 (−24,−50,−8)/3.6 (36,−36,−11)
	Middle temporal gyrus	22, 21	3.8/0.1	4.0 (−56,−35,−1)/2.6 (48,−32,2)
	Middle frontal gyrus	6	0.4/NA	4.0 (−30,−12,45)/NA
Negative phase (only phase)	Superior temporal gyrus	41, 22, 42, 21	2.3/3.4	4.0 (−53,−34,10)/3.9 (45,−34,13)
	Postcentral gyrus	2	NA/0.1	NA/3.8 (50,−30,35)
	Transverse temporal gyrus	41	0.0/0.2	2.6 (−50,−26,10)/3.7 (45,−31,13)
	Lingual gyrus	18	0.5/0.6	3.0 (−21,−87,−1)/3.5 (18,−88,−3)
	Basal ganglia		0.3/0.2	3.0 (−24,−15,−2)/2.9 (30,−18,−4)
	Thalamus		NA/0.0	NA/2.9 (15,−17,17)
	Insula		0.1/NA	2.7 (−30,1,17)/NA
	Inferior occipital gyrus	18	0.1/NA	2.7 (−30,−82,−3)/NA
	Supramarginal gyrus		NA/0.1	NA/2.6 (45,−36,35)
	Anterior cingulate		0.1/NA	2.5 (−12,29,−6)/NA
Positive phase (only phase)	Precentral gyrus	43, 6, 13, 9	1.3/0.1	4.0 (−39,−19,34)/2.8 (39,−10,39)

	Area	Brodmann area	L/R volume	L/R random effects, max *T* (*x*, *y*, *z*)
	Postcentral gyrus	3, 2	1.0/NA	3.7 (−39,−16,31)/NA
	Middle frontal gyrus	6	0.2/1.3	2.8 (−33,6,52)/3.6 (27,6,55)
	Precuneus	7, 31	0.6/0.2	3.2 (−15,−50,49)/2.7 (3,−59,44)
	Cingulate gyrus	31	0.2/0.1	3.2 (−15,−42,27)/2.8 (12,−42,27)
	Superior temporal gyrus	22	0.1/0.0	2.6 (−50,−3,3)/2.9 (50,−11,9)
	Posterior cingulate		NA/0.0	NA/2.8 (12,−42,24)
	Medial frontal gyrus		NA/0.2	NA/2.8 (21,5,49)
	Insula		0.1/0.0	2.6 (−45,−11,17)/2.5 (36,−8,11)
	Middle temporal gyrus		0.0/NA	2.5 (−42,−61,3)/NA
	Paracentral lobule	5	NA/0.0	NA/2.5 (18,−41,55)
	Superior frontal gyrus		NA/0.0	NA/2.5 (30,11,49)

Table 6

MNI table for RGB maps of auditory oddball.

	Area	Brodmann area	L/R volume	L/R random effects, max *T* (*x*, *y*, *z*)
Magnitude (magnitude and phase)	Superior temporal gyrus	21, 22, 42, 41, 13, 38, 39	5.5/4.0	8.9 (−56,−12,−2)/8.2 (59,−29,10)
	Insula	13, 47	1.0/1.0	5.8 (−56,−37,18)/7.3 (45,−15,−2)
	Inferior frontal gyrus	45, 47, 13, 9	2.2/0.9	7.2 (−45,24,13)/5.5 (45,18,10)
	Middle temporal gyrus	21, 22, 39	1.0/0.8	7.0 (−50,−38,5)/4.3 (53,−43,8)
	Transverse temporal gyrus	41	0.0/NA	5.3 (−53,−23,12)/NA
	Caudate		0.2/NA	5.2 (−12,−2,19)/NA
	Middle frontal gyrus	9	0.2/0.0	5.1 (−45,8,38)/3.7 (42,22,24)
	Inferior parietal lobule	40	0.7/0.1	4.9 (−62,−37,24)/3.7 (53,−40,24)
	Postcentral gyrus	40	0.2/NA	4.9 (−56,−25,15)/NA
	Precentral gyrus	6, 9	0.3/NA	4.3 (−50,−8,6)/NA
	Supramarginal gyrus	40	0.3/0.0	3.5 (−53,−36,32)/3.1 (56,−46,22)
	Parahippocampal gyrus		NA/0.1	NA/3.5 (33,−9,−15)
	Cingulate gyrus		0.1/NA	3.3 (−12,−4,28)/NA
	Superior frontal gyrus	6	NA/0.0	NA/3.0 (3,6,52)
Magnitude (only magnitude)	Superior temporal gyrus	22,21,41,38,42,13,39	21.4/18.8	10.7 (−59,−20,1)/8.2 (56,−29,10)
	Middle temporal gyrus	21,22,38,39	12.5/5.7	9.8 (−48,−21,−4)/7.2 (50,−18,−4)
	Transverse temporal gyrus	41,42	1.5/1.8	5.8 (−45,−29,10)/7.5 (45,−31,13)
	Insula	13,22,47,41,40,45	4.2/7.3	6.9 (−42,−20,1)/7.3 (45,−15,−2)
	Inferior frontal gyrus	9,45,46,47,13,44,10	14.9/5.6	7.0 (−48,24,13)/5.5 (39,20,−1)
	Middle frontal gyrus	46,6,9,8,10	18.6/5.8	6.9 (−45,16,27)/5.4 (39,16,27)
	Postcentral gyrus	40,43	1.0/1.7	6.1 (−65,−23,15)/6.6 (56,−25,15)
	Cuneus	17,18	2.3/1.3	5.8 (−15,−93,0)/4.4 (3,−93,0)
	Lingual gyrus	17,18	3.2/1.6	5.6 (−18,−93,−3)/4.7 (3,−87,−1)
	Cerebellum		0.1/6.1	5.0 (−53,5,44)/5.4 (15,−80,−24)
	Medial frontal gyrus	8,6,32	2.2/0.9	5.4 (−6,20,46)/4.4 (3,17,46)
	Precentral gyrus	44,6,9,13	1.1/0.6	5.0 (−53,5,44)/5.3 (45,18,7)
	Superior frontal gyrus	6,8,10,9	6.0/1.0	5.3 (−6,14,49)/4.6 (3,17,49)
	Caudate		0.4/1.2	4.9 (−9,4,16)/5.0 (9,4,16)
	Inferior parietal lobule	40	2.1/1.7	4.9 (−62,−37,24)/4.3 (45,−34,24)
	Parahippocampal gyrus		0.5/0.6	4.5 (−33,−4,−17)/4.6 (27,−9,−12)
	Thalamus		3.2/1.1	4.6 (−12,−9,3)/4.3 (6,−9,0)
	Basal ganglia		1.4/0.3	4.5 (−12,6,−5)/ 4.4 (36,−20,4)
	Cingulate gyrus	32,23	1.3/0.8	4.2 (−12,−2,28)/4.1 (3,−22,26)
	Supramarginal gyrus	40	0.3/NA	3.8 (−62,−46,22)/NA
	Inferior temporal gyrus	21	0.1/NA	3.6 (−56,−7,−15)/NA
	Posterior cingulate	23	NA/0.1	NA/3.5 (3,−28,24)
	Anterior cingulate	33	NA/0.0	NA/3.4 (6,10,22)
	Uncus	28	0.1/0.1	3.1 (−30,−1,−20)/3.2 (30,5,−20)
	Inferior occipital gyrus	17	0.1/NA	3.1 (−21,−97,−8)/NA

	Area	Brodmann area	L/R volume	L/R random effects, max *T* (*x*, *y*, *z*)
Negative phase (magnitude and phase)	Superior temporal gyrus	22, 13, 39, 41, 42, 21, 38	5.5/3.3	5.7 (−48,−40,13)/8.0 (50,−46,13)
	Middle temporal gyrus	21, 39, 22	1.0/0.8	4.4 (−48,−41,2)/4.7 (53,−46,8)
	Insula	13, 47	1.0/0.3	4.3 (−45,−40,19)/3.4 (39,21,13)
	Inferior frontal gyrus	45, 47, 13, 9	2.2/0.9	4.0 (−39,2,30)/4.0 (42,21,13)
	Precentral gyrus	6, 9	0.3/NA	3.6 (−39,1,28)/NA
	Inferior parietal lobule	40	0.7/0.1	3.5 (−56,−37,24)/3.3 (50,−40,24)
	Caudate		0.2/NA	3.3 (−12,−2,17)/NA
	Postcentral gyrus	40	0.2/NA	3.1 (−53,−23,15)/NA
	Cingulate gyrus		0.1/NA	2.9 (−15,−4,28)/NA
	Transverse temporal gyrus	41	0.0/NA	2.7 (−53,−23,12)/NA
	Supramarginal gyrus	40	0.3/0.0	2.5 (−50,−39,35)/2.2 (56,−46,22)
	Superior frontal gyrus	6	NA/0.0	NA/2.3 (3,6,52)
	Middle frontal gyrus	9	0.2/0.0	2.2 (−48,5,36)/2.1 (42,22,24)
Positive phase (magnitude and phase)	Superior temporal gyrus	22	NA/0.7	NA/3.7 (36,−1,−15)
	Insula	13	NA/0.7	NA/3.5 (39,−17,4)
	Parahippocampal gyrus		NA/0.1	NA/3.3 (33,−4,−15)
Negative phase (only phase)	Superior temporal gyrus	13, 39	0.4/0.6	4.0 (−39,−40,10)/6.5 (48,−46,19)
	Inferior parietal lobule	40	0.9/0.6	3.6 (−53,−42,24)/5.8 (48,−46,22)
	Supramarginal gyrus	40	1.1/0.2	4.3 (−50,−45,30)/4.1 (50,−48,22)
	Inferior frontal gyrus	6, 9, 46	0.3/0.8	3.8 (−39,−1,30)/3.5 (36,29,7)
	Precentral gyrus	6	0.4/NA	3.6 (−42,1,28)/NA
	Insula	13	0.7/NA	3.3 (−42,−40,19)/NA
	Middle temporal gyrus	37, 21, 39	0.2/0.4	3.3 (−39,−43,8)/3.3 (65,−53,−2)
	Middle frontal gyrus	11, 46, 47	NA/0.3	NA/3.0 (36,41,−5)
	Inferior temporal gyrus	37	NA/0.0	NA/2.7 (65,−53,−5)
	Cingulate gyrus		0.0/NA	2.7 (−15,−4,31)/NA
	Postcentral gyrus		0.1/NA	2.5 (−53,−22,18)/NA
	Basal ganglia		0.1/NA	2.5 (−30,12,−1)/NA
Positive phase (only phase)	Parahippocampal gyrus		NA/0.1	NA/3.2 (33,−7,−17)
	Insula		NA/0.2	NA/2.9 (39,−14,6)
	Basal ganglia		NA/0.1	NA/2.8 (36,−17,4)
	Superior temporal gyrus		NA/0.1	NA/2.3 (45,5,−20)
	Middle temporal gyrus	21	NA/0.1	NA/2.3 (42,4,−28)